ELSEVIER

Biochimica et Biophysica Acta 1364 (1998) 403–419

BIOCHIMICA ET BIOPHYSICA ACTA
BBA

Multiple crystal types reveal photosystem II to be a dimer

Mary K. Lyon *

Department of Molecular, Cellular and Developmental Biology, Campus Box 347, University of Colorado, Boulder, CO 80307, USA

Received 24 February 1998; accepted 4 March 1998

Abstract

Three types of photosystem II (PS II) crystals have been produced using a variety of detergents. Intermediate stages of crystal formation were examined and it was determined that each crystal probably originates from a single grana membrane. Each crystal type was examined by electron microscopy and image processing, providing three different projection maps. The highest resolution results came from type 1 and type 2 crystals. Projection maps from these crystals were examined for two-fold symmetry via difference maps between the unsymmetrized averages and their 180° rotation. A comparison of the final maps shows a high degree of two-fold symmetry, with only slight differences noted in the low density regions of the two halves of the structure. The interpretation is that PS II is a dimer, with the further suggestion that the two reaction center cores may have slightly different complements of antennae polypeptides.

Keywords: Photosystem II; Spinach; Structure; Electron microscopy; Two-dimensional crystal; Correlation averaging

1. Introduction

Photosystem II (PS II) is one of two reaction centers found in the photosynthetic membranes of green plants and is one of the most important membrane protein complexes known because it releases oxygen as a byproduct and is, in fact, the most vital link in the cycling of oxygen throughout the atmosphere. PS II is large, consisting of at least twenty polypeptides, chlorophylls *a* and *b* and multiple other pigments and cofactors [1–5]. The exact stoichiometry of some of the polypeptides has yet to be determined, so that the total molecular weight of an individual PS II complex remains somewhat hypothetical.

Because of this size and complexity, the structure of PS II has proven very difficult to study. There have been many publications regarding PS II structure [6–24], yet the results are in conflict, resulting in as many questions as there are answers. Each preparation method has resulted in distinctly different sizes reported for PS II. There is also a continuing controversy whether PS II exists as a monomer or dimer in vivo. Relatively similar structures are, in some cases, interpreted as a monomer with pseudosymmetry and including one PS II complex (e.g., Refs. [10,17]) and in other cases are believed to be true dimeric structures including two PS II complexes (e.g., Refs. [13,14,18,19,21,23,24]). Several reviews of the struc-

Abbreviations: FRC: Fourier ring correlation; LHC II: light-harvesting chlorophyll *a*/*b* binding complex; OEE: oxygen evolution-enhancing polypeptides; PS II: photosystem II; RC: reaction center; SSNR: spectral signal-to-noise ratio

* Corresponding author. Fax: +1-303-492-7744; E-mail: mkl@demeter.colorado.edu

0005-2728/98/$19.00
PII S0005-2728(98)00064-4

ture of photosystem II have recently been published. Two reviews propose that the monomer model is correct [25,26], but two suggest that the dimer model is more strongly supported by the current evidence [27,28].

In this report, three types of tubular crystals of PS II are examined, as well as intermediate stages of crystal formation. The issue of two-fold symmetry was examined, and it appears that the structure is indeed a dimer, but with the possibility of very subtle differences between the two monomers.

2. Materials and methods

2.1. Preparation of crystals

Crystals were prepared essentially as described [9], with modifications as noted below. Both market and greenhouse spinach were used. Several varieties of spinach were grown: Avon (Burpee), Space (Pinetree Garden Seeds), Tyee f1 (High Altitude Gardens), Nordic (Park Seeds), Bolero (Keithly–Williams Seeds) and Bossanova (Keithly–Williams Seeds). Detergents used were Triton X-100 (Sigma), dodecylmaltoside (Anatrace), tridecylmaltoside (Anatrace) and tetradecylmaltoside (Anatrace).

Briefly, thylakoids were isolated in buffer *A*, washed in buffer *B*, and resuspended in buffer *C* to a chlorophyll concentration of 0.8 mg/ml, as before [9]. The first detergent treatment was done for 20 min on ice with stirring. The detergent ratios and percentages were: Triton X-100 (4.5:1, 0.36%) or dodecylmaltoside (1:1, 0.08%). Each sample was treated with one detergent, not a mix of detergents. The membranes were then centrifuged, resuspended in buffer *D*, centrifuged once again and resuspended in buffer *B*, as described [9]. For the second detergent treatment, the chlorophyll concentration was 2.0 mg/ml and the detergent ratios and percentages were: Triton X-100 (3:1, 0.6%), dodecylmaltoside (1:1, 0.2%), tridecylmaltoside (1:1, 0.2%) or tetradecylmaltoside (1:1, 0.2%), with treatment for 10 min on ice. The suspensions were then washed and differential centrifugation used, as described previously [9].

2.2. Electron microscopy and image-processing

Low-dose images were obtained as described [9]. The type 3 crystal images were obtained by searching at a higher magnification and were not low-dose. Correlation averaging was done as previously described [9,13]. For Fourier averaging, SPECTRA, version 3.0 [29] was installed and used on a Silicon Graphics workstation (SGI O2 with a 180 MHz R5000 CPU, running IRIX 6.3).

3. Results

3.1. Description of crystal types and crystallization process

Sequential treatment of spinach thylakoid membranes with Triton X-100 detergent [9,13] yields two-dimensional (2-D) crystals and vesicles. The process involves treatment with detergent washes and a second treatment with detergent. Biochemical evidence suggests that these crystals include D1, D2, cytochrome *b*-559, CP47, CP43, CP29, CP26, CP24 and CP22 [13]. In order to improve on the quality of the crystals, a variety of detergents have been used and three crystal types have been found (Fig. 1). The three crystal types are distinguished by having unique unit cells, and not by the detergents used to produce them. In fact, in two cases, different detergents could be used to produce the same type of crystal.

Type 1 crystals (Fig. 1a) can be produced with Triton X-100 or three types of maltoside detergents (dodecylmaltoside, tridecylmaltoside or tetradecylmaltoside) as the secondary detergent, but all require that Triton X-100 be used for the first detergent treatment. The maltoside detergents generally provided better resolution. Grooves were visible at an angle relative to the longitudinal axis of the tube (arrow, Fig. 1a). The grooves are most visible when the images are viewed at a glancing angle. Weaker grooves were also found in the opposite direction (arrowhead, Fig. 1a). Type 2 crystals (Fig. 1b) could be obtained only with the use of maltoside detergents as the secondary detergent. Both type 1 and type 2 crystals were found in each preparation. The type 2 crystals were variable in length and narrower (about 175 nm flattened width) than the type 1 crystals. Very rarely, a crystal could be found where there was an abrupt change in width and a switch from type 1 to type 2 crystal. Type 2 crystals were characterized by prominent grooves in both directions (arrows, Fig.

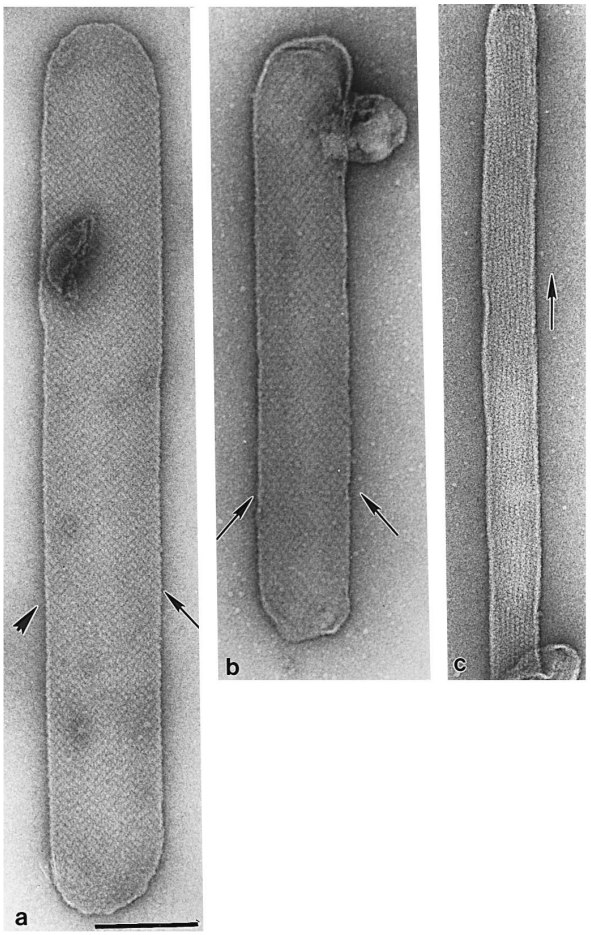

Fig. 1. Three types of negatively stained tubular crystals of PS II. (a) Type 1 crystal, found with both TX-100 and maltoside detergents. Predominant grooves (arrow), weaker grooves (arrowhead). (b) Type 2 crystal, found only with the maltoside detergents as the secondary treatment. Arrows indicate grooves. (c) Type 3 crystal, found very rarely with TX-100 as the secondary detergent. The grooves (arrow) are almost parallel to the longitudinal axis of the tube. Bar = 200 nm and applies to all crystal types.

1b). Type 3 crystals (Fig. 1c) were extremely rare. Type 3 crystals, found only with Triton X-100 as the secondary detergent, were characterized by being extremely narrow (about 100 nm), though again, with variable length. Grooves were nearly parallel to the longitudinal axis of the tube (arrow, Fig. 1c). Unlike the situation with the maltoside detergents, either type 1 or type 3 crystals were found when Triton X-100 was used as the secondary detergent, but not both in the same preparation.

The preparations produced tubular crystals, incompletely formed crystals and vesicles (Fig. 2). Obser-

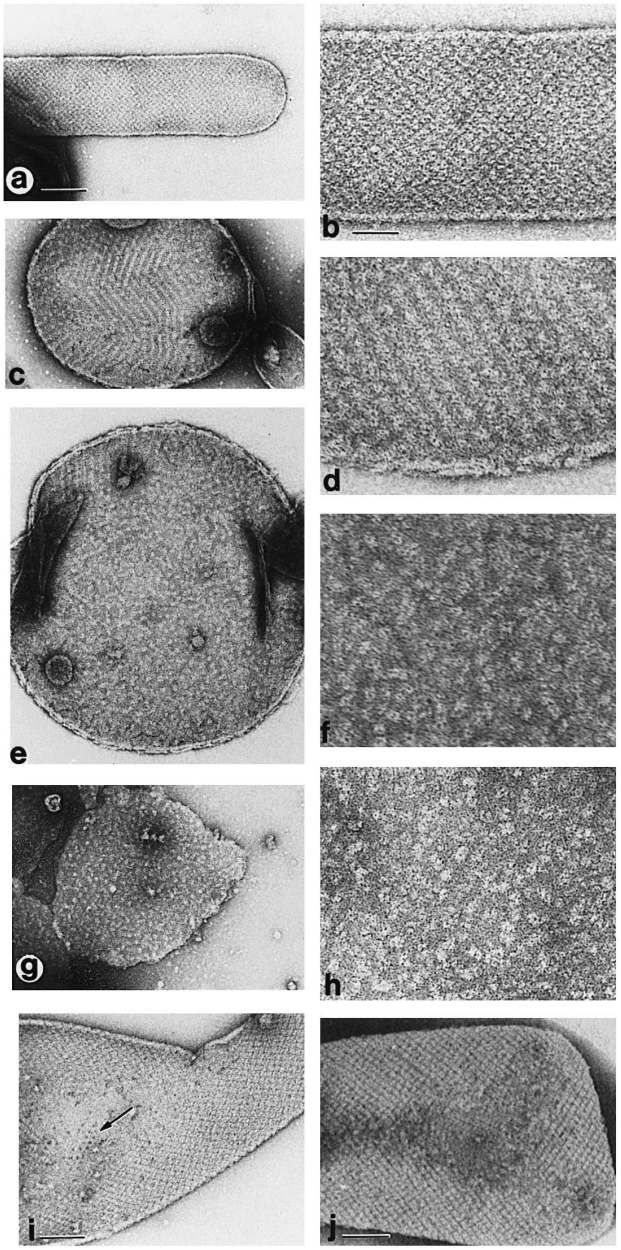

Fig. 2. Intermediate stages in the formation of tubular crystals. (a) and (b) An example of a tubular type 1 crystal. (c–f) Vesicles characteristic of those found in the preparations of tubular crystals. Rows of aligned particles were frequently found (c) and (d). (g) and (h) Grana fragments, known to consist of the stacked portions of grana, with the particles identified as PS II [30,31]. There is a clear similarity of the surfaces in (f) and (h). (i) and (j) Tubular crystals were sometimes found with bulbous ends and multiple incipient tubular crystals. In the center of the bulb region, a hexagonal pattern of holes is apparent (arrow). (a) Bar = 120 nm and applies to (a), (c), (e), (g). (b) Bar = 45 nm and applies to (b), (d), (f), (h). (i,j) Bar = 75 nm.

vation of incompletely formed crystals and vesicles, which were separated from the tubular crystals by differential centrifugation, suggests some possible mechanisms for crystal formation. The surface of vesicles found in the crystal preparations (Fig. 2c–f) was similar in appearance to the surface of grana-derived membrane fragments (Fig. 2g–h), which are known to consist of inside-out grana membrane fragments [30]. The multimeric particles found on the surface consist of PS II [31]. Thus, the vesicles found in the crystal preparations appear to be relatively intact, inside-out grana. It was frequently found that individual particles were in rows in these vesicles (Fig. 2c–d). Rows were arranged in areas with a width of approximately 200 nm, the same width as completely formed type 1 crystals. Rows forming a

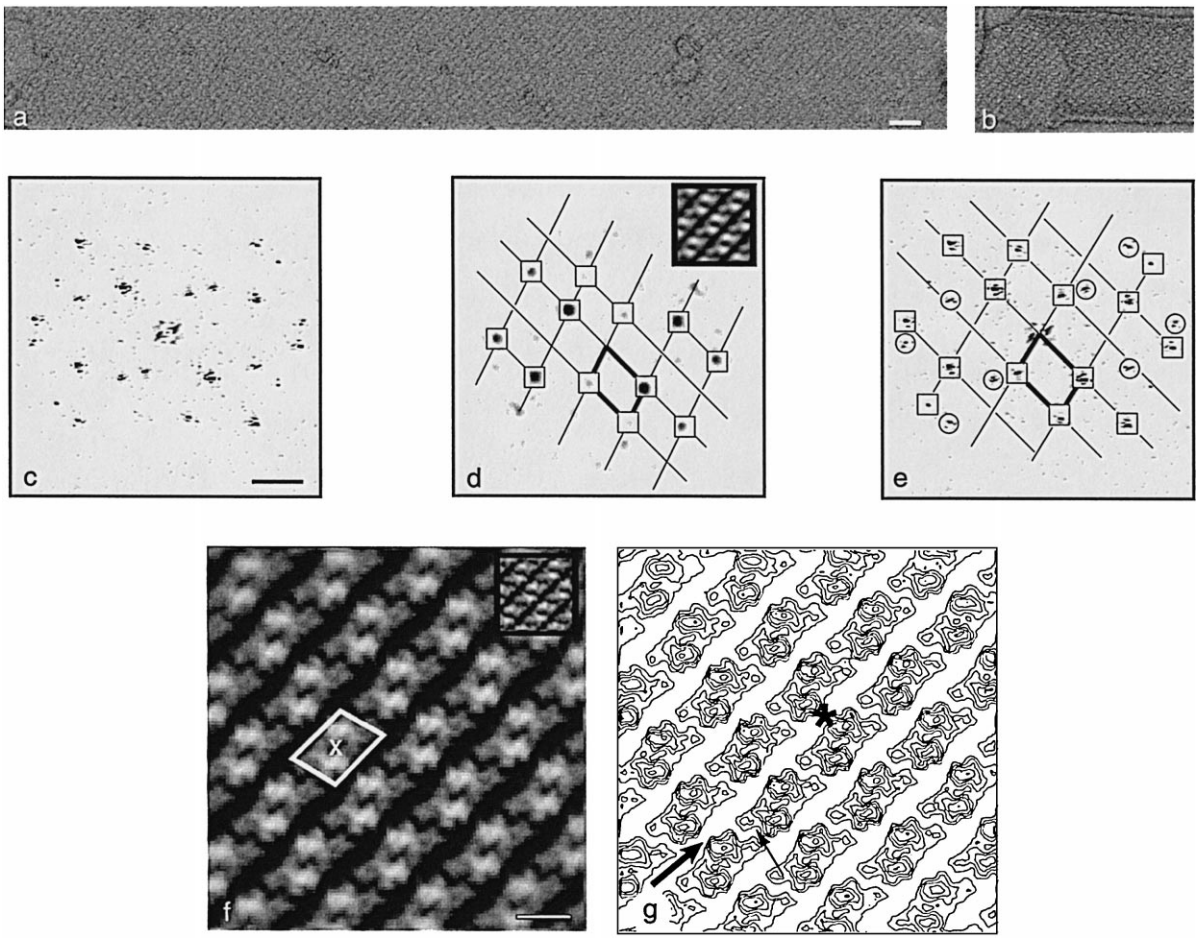

Fig. 3. Type 1 crystals. (a) Low-dose image of type 1 crystal. Bar = 50 nm and applies to both (a) and (b). (b) High-dose image of a ripped crystal, with a single layer present in the ripped portion. (c) Partial power spectrum from 256 × 256 pixel area of (a). Bar = 1/10 nm and applies to (c), (d), (e). (d) Power spectrum from 128 × 128 pixel area of the ripped portion in (b). Unit cell is indicated by solid lines. Inset shows average obtained by Fourier averaging of this power spectrum. (e) Power spectrum as in (c), but with indexing indicated. Reflections with boxes are from the strongly diffracting side and those with circles are from the opposite side of the crystal. (f) Density map obtained from a single tube (810 peaks). SSNR resolution was 1.8 nm; FRC resolution was 1.2 nm. The unit cell (16.8 × 11.9 nm) is outlined, with *X* indicating a central cleft with apparent two-fold rotational symmetry. This map has not been filtered, nor has symmetry been imposed. Inset shows a density map obtained from the ripped portion via correlation averaging, averaging only 55 peaks with a SSNR resolution of 3.8 nm. Bar = 10 nm and also applies to (g). (g) Contour map derived from (f). Contours were done to emphasize the positive densities and show the relationship of the apparent dimeric particles. The major groove is indicated by the large arrow, while the minor groove is indicated by the small arrow. The rows of particles are staggered, so that high density areas from neighboring rows are directly opposite each other (∗).

wide sheet were never found. Vesicles which had more than one partially formed crystal invariably had a central area devoid of particles (Fig. 2i–j). Separation into LHC II (light-harvesting chlorophyll *a/b* complex)-enriched and PS II-enriched areas within single vesicles also seemed to be occurring, as small patches of hexagonally arranged holes were frequently found in the same membrane with incipient PS II crystals (Fig. 2i). The hexagonally arranged holes are characteristic of two-dimensional crystals of LHC-II [32].

Market spinach was used for many of the preparations. However, it has been found that it is difficult to obtain crystals in the summer, while exceptional yields are obtained in the winter. To circumvent these problems, several varieties of spinach were grown in a greenhouse under natural light conditions. Some varieties of spinach (Avon, Bolero) were more likely to produce crystals. However, even the Avon variety gave varying results throughout the year, with winter being the most likely time to obtain crystals.

3.2. Individual projection maps from the three types of crystals

For image processing, low dose images were collected of negatively stained type 1 and type 2 crystals, while, because they were rare, only high dose images were obtained of the type 3 crystals. Fig. 3 shows a portion of a low-dose image of a negatively stained type 1 crystal (Fig. 3a) with its accompanying power spectrum (Fig. 3c). Because the tubes are flattened, the power spectrum contains a pattern from both the top and the bottom layers. High-dose images of ripped tubes were also examined (Fig. 3b) and the power spectra of this single layer was indexed (Fig. 3d). The examination of the ripped tubes allowed comparison of the results from one layer with results from two layers. The final indexing used on the intact type 1 crystals is shown in Fig. 3e. One side (lines, Fig. 3e) gave a stronger pattern, but the opposite side (circled reflections) gave a sufficiently strong pattern to indicate the unit cell. After indexing and filtering the stronger side, a reference image was produced and used for cross-correlation to obtain a projection map derived from one side only.

The projection map from a single crystal formed with dodecylmaltoside as the second detergent is shown as a density (Fig. 3f) and a contour map (Fig. 3g). The inset in Fig. 3f is a density map derived from the single-layer high-dose image, with a resolution of only 3.8 nm due to the limited number of unit cells in the ripped area, but the structure is clearly similar to that shown in Fig. 3f. Both maps were obtained via correlation averaging, while the map shown in the inset of Fig. 3d was obtained via Fourier averaging. The maps have not been filtered, nor has symmetry been imposed. The unit cell ($16.7 \pm 0.3 \times 12.0 \pm 0.2$ nm, angle 75.7 ± 3.0, Table 1) was determined from the power spectrum and is indicated on the density map. The unit cells varied only slightly with the use of different detergents

Table 1
Crystal types

Detergents (# of tubes averaged)	Type	Unit cell (nm) and angle	*a/b* Ratio
TX-100, TX-100 (5)	1	$16.8 \pm 0.2 \times 11.8 \pm 1$ 75.3 ± 1.5	1.43 ± 0.02
TX-100, dod. (7)	1	$16.7 \pm 0.3 \times 12.0 \pm 0.2$ 75.7 ± 3.0	1.40 ± 0.04
TX-100, tetra. (5)	1	$16.7 \pm 0.1 \times 12.0 \pm 0.3$ 75.3 ± 2.0	1.39 ± 0.03
TX-100, dod. (5)	2	$16.5 \pm 0.6 \times 15.7 \pm 0.7$ 69.1 ± 2.0	1.06 ± 0.07
TX-100, tetra. (5)	2	$16.4 \pm 0.6 \times 15.1 \pm 0.3$ 69.6 ± 1.0	1.08 ± 0.04
TX-100, TX-100 (4)	3	$15.6 \pm 0.3 \times 10.8 \pm 0.4$ 74.2 ± 8.9	1.44 ± 0.06

TX-100 = Triton X-100, dod. = dodecylmaltoside, tetra. = tetradecylmaltoside. Note: type 3 was from high-dose images.

(Table 1). Each unit cell encloses an apparent dimer, with two-fold rotational symmetry about a single point (*X*, Fig. 3f). The dimers are arranged in staggered rows. Densely staining grooves separate these rows with a space of 3.4 nm at the narrowest point and 5.2 nm at the widest point. The dimers of opposing rows are closest at the highest density regions, (star, Fig. 3g). The darkly staining grooves between the rows of dimers (large arrow, Fig. 3g) correspond to the most apparent grooves in the type 1 crystals and have an angle of 45° relative to the longitudinal axis of the tube. The arrangement of low density areas would appear to correspond to the weaker grooves and has an angle of 30° (small arrow, Fig. 3g) relative to the longitudinal axis of the crystal.

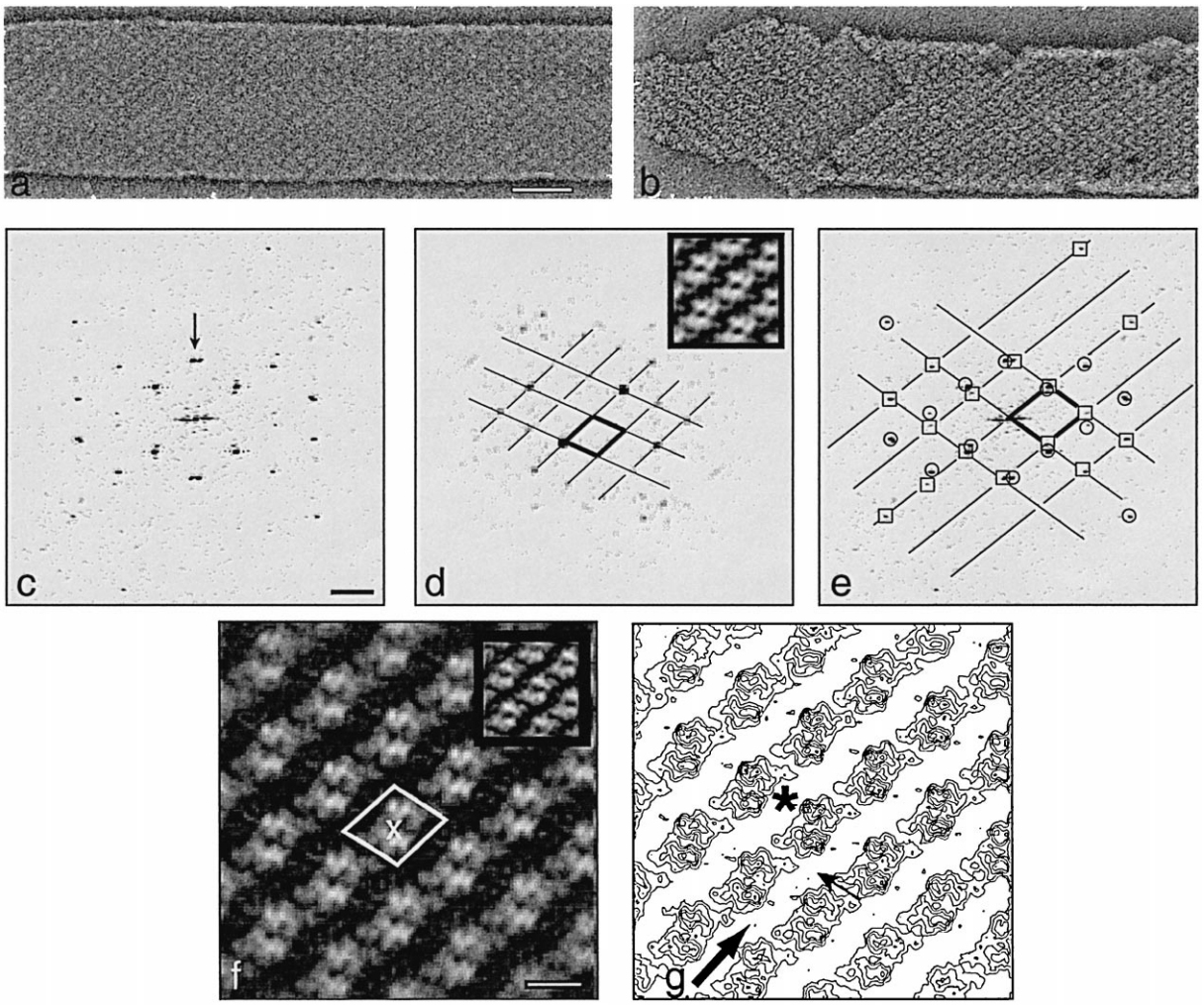

Fig. 4. Type 2 crystal derived with dodecylmaltoside as the secondary detergent. (a) Low-dose image of type 2 crystal. Bar = 50 nm and applies to (a) and (b). (b) High-dose image of ripped type 2 crystal. (c) Power spectra derived from intact tubular crystal. Arrow indicates reflections from the two sides which were frequently close together or overlapping. Bar = 1/10 nm. (d) Power spectra from ripped portion. Unit cell is indicated. Inset, Fourier average from ripped portion. (e) Indexed power spectra from intact tube. Unit cell from the dominant layer (boxed reflections) is outlined. Circled reflections are from the opposite side of the crystal. (f) Density map from single crystal (295 peaks). SSNR resolution of 2.0 nm; FRC resolution of 18.8 nm. Unit cell (16.6 × 15.2 nm) is outlined and the central cleft indicated by *X*. Inset shows map from ripped portion derived by correlation averaging, including 81 peaks and with a resolution of 2.8 nm. Bar = 10 nm and applies to (f) and (g). (g) Contours derived from (f), with positive densities emphasized. The major groove is indicated by the large arrow, while the minor groove is indicated by the small arrow. Because the rows are aligned in the type 2 crystals, heavy densities of one row are aligned with lower densities from the neighboring row (∗).

The type 2 crystals were examined in exactly the same manner (Fig. 4). The data shown are again from a single crystal, also with dodecylmaltoside as the secondary detergent and with no symmetry imposed. The unit cell ($16.5 \pm 0.6 \times 15.7 \pm 0.7$ nm, angle 69.1 ± 2.0) is indicated on the density map (Fig. 4f) and in Table 1. As with the type 1 crystals, the map shows apparent dimers arranged in rows. However, in the type 2 crystals, the rows are not staggered, so that the apparent dimers are aligned in both directions, resulting in a near-hexagonal arrangement with a central apparent dimer. In contrast to the type 1 crystals, high density regions of the apparent dimers in one row are aligned with low density regions of the next dimer (star, Fig. 4g). There is a densely staining groove with a width of approximately 7.2

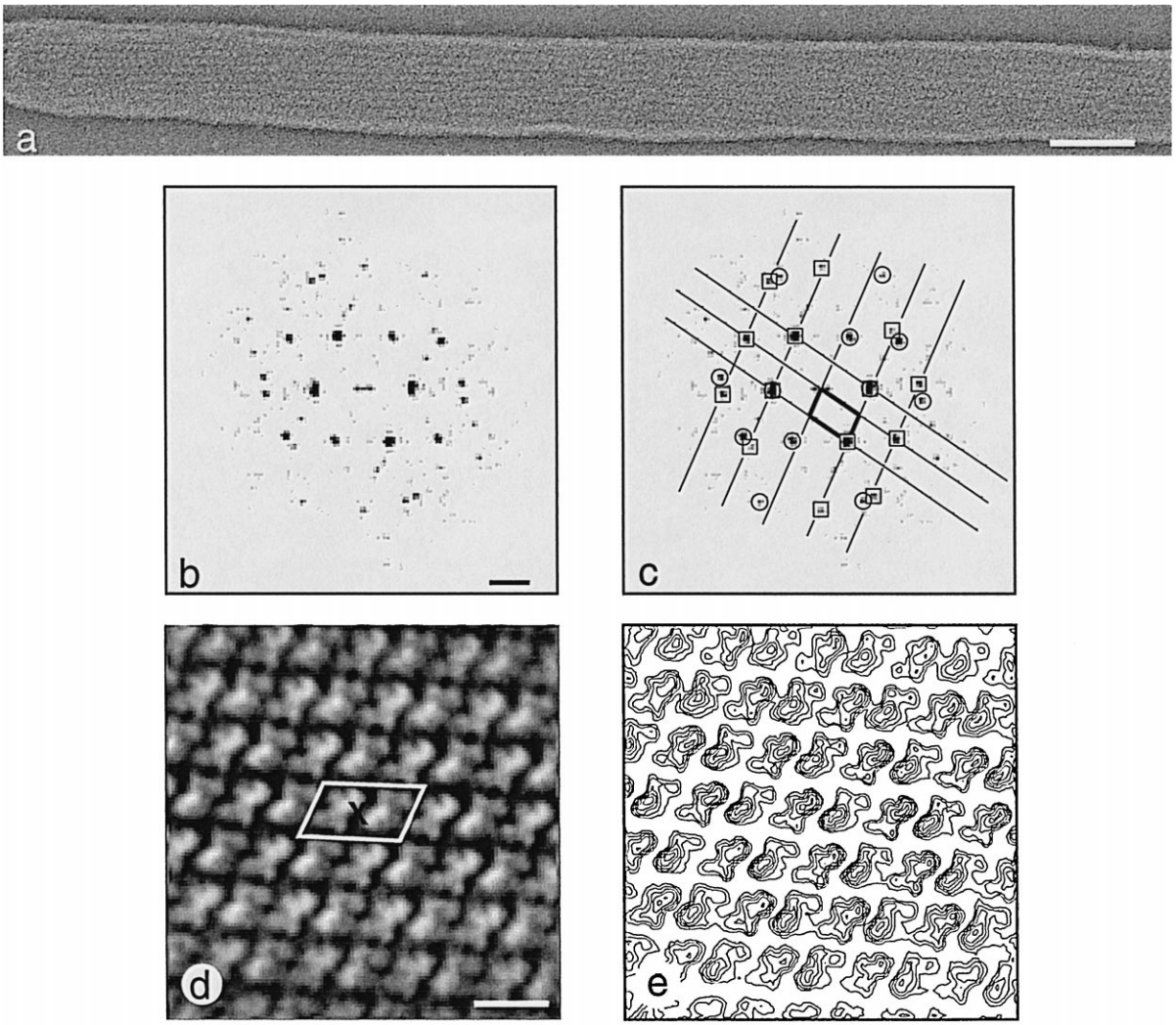

Fig. 5. Type 3 crystals. (a) High-dose image of negatively stained type 3 crystal. Bar = 100 nm. (b) Power spectra of type 3 crystal. Bar = 1/10 nm. (c) Power spectra as in (b) with indexing indicated. Reflections with boxes are from the strongly diffracting side; those with circles are from the opposite side. Several of the reflections from the opposing sides are closely spaced, making separation in Fourier space difficult. (d) Density map with unit cell (16.4×11.0 nm) outlined and central cleft indicated by *X*. The resolution was 3.0 nm based on SSNR; 2.5 nm based on FRC. No symmetry has been applied. Bar = 12 nm and applies to both (d) and (e). (e) Contour map of the average in (d). The major groove has an angle of only 3–4° with respect to the longitudinal axis of the tubular crystal.

nm, which is considerably wider than that found in the type 1 crystals. The angle of this groove (large arrow, Fig. 4g) is approximately 60° relative to the longitudinal axis of the tube. In contrast to type 1 crystals, there is a more obvious secondary groove, also with an angle of about 60° (small arrow, Fig.

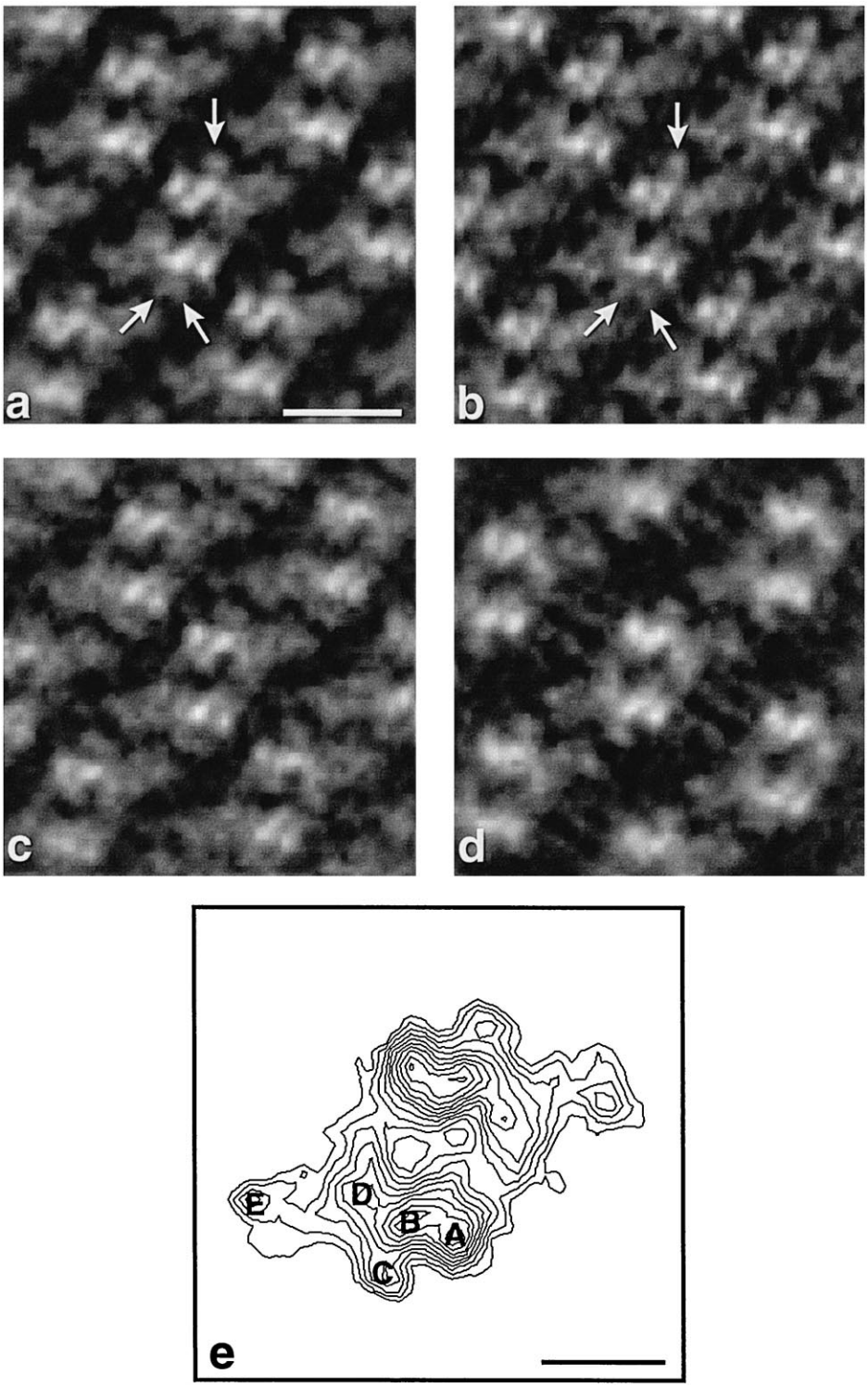

4g). In addition, there is an indication of some very low density materials within the major grooves (Fig. 4f).

The third type of crystal was found only occasionally. In spite of sometimes being quite long (Fig. 5a), these crystals always gave relatively poor resolution, so will only briefly be described. A power spectra is shown in Fig. 5b, with the indexing shown in Fig. 5c. The unit cell was $15.6 \pm 0.3 \times 10.8 \pm 0.4$ nm, with an angle of $74.2 \pm 8.9°$ (Table 1) and is indicated by solid lines on the density map (Fig. 5c). While the resolution is poor (SSNR 3.0 nm; FRC 2.7 nm), roughly dimeric units arranged in rows are visible. The rows are staggered as in crystal type 1, so that heavy density regions of neighboring rows are again in close approximation. Unlike the type 1 crystals, the rows are nearly parallel to the longitudinal axis of the crystals, with an angle of about 4°.

3.3. Separation of layers, two-fold symmetry and resolution tests

As a further check of the separation of the two layers to obtain a final average, a single type 1 crystal derived with tetradecylmaltoside was processed in two ways: correlation averaging and Fourier averaging. Correlation averaging involves alignment and averaging of densities in real space. Unit cells of the opposite layer should not be aligned, and thus, not contribute to the final average (e.g., Ref. [33]). Fourier averaging involves masking the reflections of the diffraction pattern from one side, while blocking the reflections from the opposite side, thus providing an average unit cell derived from one side only (e.g., Ref. [34]). The results are presented in Fig. 6, where (a) was derived via correlation averaging and (b) via Fourier averaging. The unit cell for Fig. 6a was 16.8×11.8 nm and for (b) was 15.7×11.4 nm. The results in Fig. 6a involve some selection, as unit cells which showed large deviations in rotation or translation were eliminated. No corrections for tilt were applied to Fig. 6b, so that this average should be considered as raw data. In both cases, symmetry has not been applied. The number of unit cells included in the average for Fig. 6a was 481; a 512×256 pixel area (approximately 307×154 nm) was used to obtain the average in Fig. 6b. Thus, although both maps came from the same tubular crystal, they are not averages of precisely the same unit cells.

Regardless of the method of averaging, five main areas of density were observed (*A–E*, Fig. 6e), in agreement with previous results [14]. While there is an obvious indication of two-fold symmetry about the central cleft, there were differences between the two halves of the apparent dimer, regardless of which method of averaging was used. These differences were most notable in the lower density areas. Area *C* showed the strongest difference, where there appeared to be one density on one side and two densities on the opposite side (arrows, Fig. 6b). Similar differences have been noticed previously with cryo-electron microscopy [13], where no stain was present. For comparison, similar projection maps derived by correlation averaging are shown from a type 1 crystal derived with dodecylmaltoside (Fig. 6c) and a type 2 crystal, also derived with dodecylmaltoside (Fig. 6d). Again, these maps have not been filtered, nor has symmetry been imposed. As with the maps in Fig. 6a and b, there are subtle differences between the two halves of the apparent dimer, but the primary struc-

Fig. 6. Single crystal averages derived by different methods. No symmetry was applied to any of the averages. (a) Average obtained via correlation averaging from a type 1 crystal derived with dodecylmaltoside. Resolution of 1.8 nm (SSNR); 1.1 nm (FRC). Bar = 10 nm and applies to (a), (b), (c) and (d). (b) Average obtained by Fourier averaging from the same crystal as used for (a). Resolution was 1.2 nm, based on the furthest reflection with an IQ of 4 or better. No corrections for tilt were made on the Fourier average (b), but unit cells requiring a high degree of rotation or shift were eliminated from the correlation averages (a,c,d). There are some differences between the averages derived by different methods (a and b) due to both resolution differences and amount of selection involved. However, the structures derived by the two methods are clearly very similar. (c) Correlation average from a single type 1 crystal derived with dodecylmaltoside. Resolution: (SSNR 2.1 nm; FRC 1.9 nm). (d) Correlation average from a type 2 crystal derived with dodecylmaltoside. Resolution: (SSNR 2.2 nm; FRC 1.9 nm). (e) Contour map derived from (d). Bar = 50 nm. In all cases, an apparent dimer was observed with a central cleft or hole. Each half of the dimer could be further subdivided into five areas (*A–E*, a). The three averages derived by the same methods (a,c,d) show the subtle differences observed from crystal to crystal.

ture appears similar. For example, area *C* appears identical in both halves of the apparent dimer in some cases (Fig. 6d). It is also notable that the degree of differences between the two halves of each dimer varies with each crystal, with the maps in Fig. 6d and e showing the greatest degree of similarity between the two halves.

Because there were some variations from one half of the apparent dimers to the other, each average was tested for symmetry by rotating it 180° and producing difference maps. This was done only for the type 1 and 2 crystals. Each average was filtered to 1.8 nm so that they were comparable. Examples of the results for the type 1 crystals derived with tetradecylmaltoside as the secondary detergent are shown in Fig. 7. The most pronounced differences between the two halves of the apparent dimer were generally in the low density areas, as noted previously. However, there were no consistent differences between the two halves from crystal to crystal, as indicated by the examples of difference maps (Fig. 7a–c). Locations of some of the differences are shown in the insets. The strongest differences tended to involve the low density area, *C* (Fig. 6a).

Resolution was determined by three methods, primarily because different methods of determining resolution have been used for the various studies of PS II structure and it is consequently difficult to compare results. The three methods that have been used are: reflections in the power spectrum [10,15,17,22,23], Fourier ring correlation (FRC) [12] and spectral signal-to-noise ratio (SSNR) [13,14]. The furthest reflection with an IQ rating of 4 or better indicated a resolution of 1.2 nm for the average shown in Fig. 6b, which was obtained via Fourier averaging. IQ ratings indicate the quality of the individual reflections based on signal-to-noise, with an IQ rating of 4 equivalent to a 2:1 ratio [35]. The resolution of the map in Fig. 6a, which was obtained via correlation averaging, was determined via FRC (1.1 nm) and SSNR (1.8 nm). This was one of the most extreme differences in resolution as determined by the two methods, but it clearly illustrates that different methods of determining resolution provide different results even when applied to the same sample, in confirmation of previous results with other samples [36]. The determination of resolution from the power spectrum is appropriate when the averaging is done in Fourier space. However, in the current study, the averaging has been done in real space via correlation averaging, primarily because reflections from both sides were often too close to filter for Fourier averaging. Because the resolution results differ with different methods of measurement, both FRC and SSNR results are given.

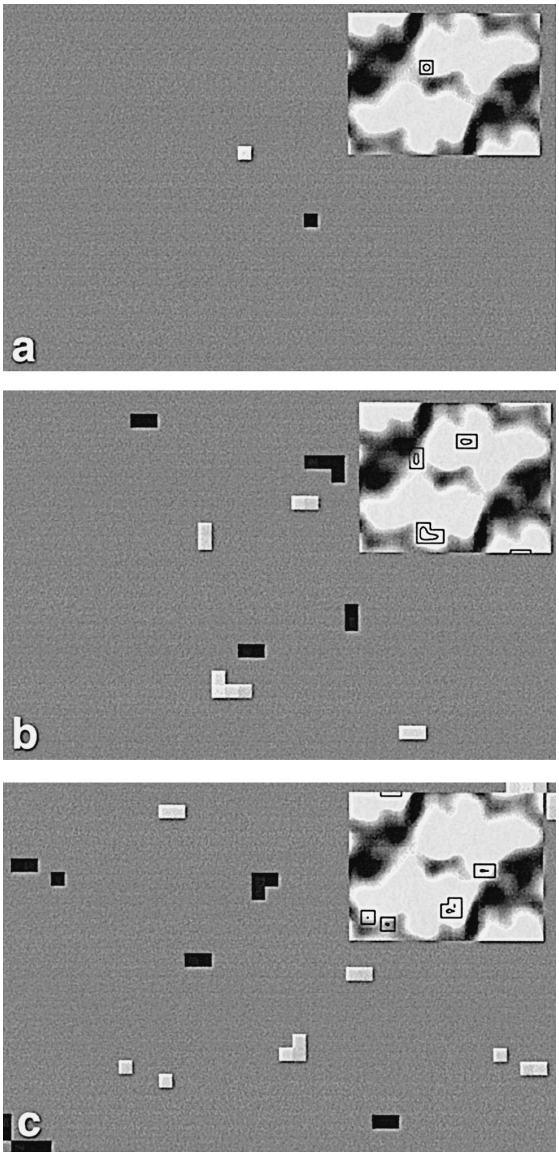

Fig. 7. Three difference maps between averages from individual crystals and their 180° rotation, with significance levels of 0.005. Insets: Positive differences (outlines) are localized on a density map. There was no consistent pattern of differences found among the crystals.

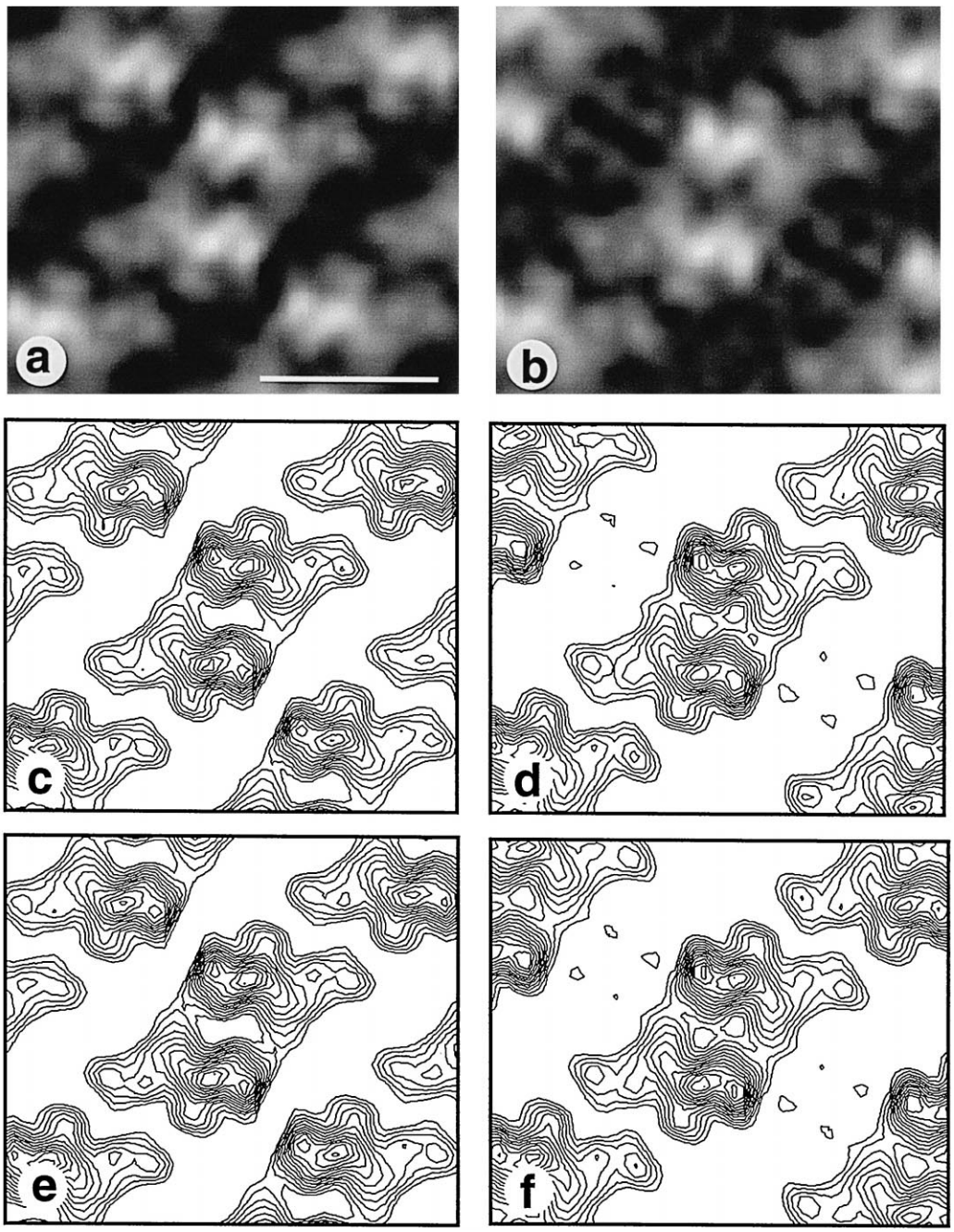

Fig. 8. Final averages from type 1 crystals (a,c,e) derived with tetradecylmaltoside as the secondary detergent and from type 2 crystals (b,d,f) with dodecylmaltoside as the secondary detergent. The average in (a) was derived from 5 crystals (1998 peaks) with a SSNR resolution of 19.9 and FRC resolution of 1.8 nm. The average in (b) was derived from 5 crystals (1212 peaks) with a SSNR resolution of 22.0 and FRC resolution of 1.9 nm. (a) and (b) Density maps with no symmetry imposed. Bar = 10 nm. (c) and (d) Contour maps with no symmetry imposed. (e) and (f) Contour maps with two-fold symmetry imposed. There is a high degree of similarity between the apparent dimers in (c) and (d), even though the structures were obtained from two different crystal types and the crystals were obtained with different detergents. Secondly, there is a high degree of apparent two-fold symmetry. Only subtle changes are observed when comparing non-symmetrized structures (c and d) with their symmetrized counterparts (e and f).

3.4. Final averages from type 1 and type 2 crystals

Final projection maps were obtained by combining data from a number of tubes of each type (Table 1). Only the final averages for type 1 crystals derived with tetradecylmaltoside and type 2 crystals derived with dodecylmaltoside are shown (Fig. 8). The averages are shown both without symmetry imposed (Fig. 8a–d) and with two-fold symmetry imposed (Fig. 8e–f). What is most striking about the two averages is that, even though they were derived from different crystal types obtained with different detergents, the apparent dimers are extremely similar. The unit cells vary primarily because of the different arrangements of these dimers, as described in Figs. 3 and 4. Both show apparent two-fold symmetry about a central depression. Two-fold symmetrized images were also produced (Fig. 8e and f), and a comparison of the non-symmetrized and symmetrized images does not show any dramatic differences.

In all cases, 5 major regions could be identified within the monomeric unit (labelled A–E, Fig. 6e). At this resolution, density *B* appears slightly higher and larger than density *A*. Also, there appears to be a projection extending into the central cleft, almost as an extension between densities, *A* and *B*. This projection narrows the gap between the two halves in the central region of the dimer. Density *C* was the area where there appeared to be the most consistent differences between the two halves of the apparent dimer, with the occasional appearance of two peaks of density in area *C* on one side of the dimer and only one peak of density on the other side of the dimer, although this difference was most notable in the type 1 crystals and not the type 2 crystals, and as stated, was not entirely consistent from crystal to crystal.

4. Discussion

PS II has proven to be one of the more difficult membrane complexes to study at the structural level, for several reasons. First, PS II includes both intrinsic and extrinsic membrane polypeptides. Secondly, PS II is quite large, consisting of multiple polypeptides. These are the obvious problems, but there are more subtle problems. Within intact thylakoids, PS II has been found to be a somewhat heterogeneous group, varying primarily with respect to the number of antennae polypeptides [37,38]. There seems to be a close functional and structural relationship between PS II and specific thylakoid lipids (e.g., Ref. [39]). Perhaps, most importantly, PS II complexes are inherently unstable, as photoinhibition studies have shown (review, Ref. [40]). While the most obvious effect of photoinhibition, whether from the donor or acceptor side, is the replacement of damaged D1 polypeptides, there is also a host of side effects which affects structure, apparent dimer to monomer transitions, loss of OEEs (oxygen evolution-enhancing polypeptides) and possible loss of antennae polypeptides. All of this evidence suggests that PS II is somewhat unstable even in its native membrane.

4.1. Formation of crystals

There was an increased ability to obtain crystals during cold weather months. One possibility for this is a change in the saturation levels of lipids closely associated with PS II. It has been found that growth at reduced temperatures affects the saturation levels of specific lipids [41]. At the same time, mutants which are deficient in desaturates have shown a tendency to form PS II crystals in the membrane [42].

While it is difficult to be certain that all of the observed variations were intermediate stages and not variant end products, those stages which had clearly identifiable tubular portions provided information regarding the crystal formation. The crystals appear to be formed by a sorting of LHC II and PS II into separate areas, specific associations developing between the PS II complexes, possibly a depletion of lipid and finally a pinching off of the PS II crystal area to form isolated tubular crystals. There are several important consequences of this purported process. First, the PS II complexes are never removed from the membranes. Second, each crystal appeared to form from PS II complexes within one grana membrane by a gradual transformation of the round shape of the grana to the tubular shape of the crystal, leaving a bulb of non-crystalline membrane at the end (Fig. 2i and [13]). A similar phenomenon has been observed in the formation of tubular crystals of other membrane proteins [34,43,44]. This last point is important with respect to the homogeneity of PS II complexes within a single tubular crystal.

All three types of crystals were tubular, regardless of the associations between the individual units or the detergents used to form them. This suggests that the curvature of the membrane is due to PS II itself. The crystals were inside-out with respect to native thylakoids, as determined by examination of metal-coated samples by AFM (atomic force microscopy) and TEM (transmission electron microscopy) [9] and in agreement with conclusions reached regarding tubular crystals obtained in an entirely different manner [23]. Thus, it is likely that the lumenal portion of PS II is wider than the stromal side of PS II, forcing the curvature. The three-dimensional structure recently obtained of dimers of D1, D2, cytochromes *b*-559, CP47 and CP43 shows a slight flaring of the structure on the lumenal side [23].

The three crystal types also revealed that PS II complexes are capable of associating in a variety of ways, suggesting that specific interactions are possible between different polypeptides within PS II. When type 1 and type 2 crystals are compared, the associations of PS II complexes within individual rows appear to be identical. In fact, rows are a common theme in almost all of the published works on PS II two-dimensional crystals [6,10,13,14,17,23]. However, across the rows, there is a distinct difference between the two crystals. In type 1 crystals, density *A* of each dimer is in close approximation with densities *A* of the neighboring row (star, Fig. 3g). In the type 2 crystals, densities *A* of one row are most closely aligned with densities *E* of the neighboring row (star, Fig. 4g).

The type 3 crystals are considerably different than the type 1 and 2 crystals but appear similar to tubular crystals formed by first removing PS II from the membranes, followed by reconstitution of these complexes with dimyristoyl phosphatidyl choline [17]. The type 3 crystals were rare and were never found in preparations in which other types of crystals were present. However, the fact that they were found at all suggests that, in some cases, PS II is susceptible to a considerable loss of polypeptides before association into crystals.

4.2. Monomer vs. dimer

Structural studies have involved several approaches—isolated complexes, isolated complexes after formation of two-dimensional crystals, and two-dimensional crystals within the membrane. The results have produced a variety of size estimates and a conflict as to whether PS II is a monomer with pseudo-two-fold symmetry or a true dimer. There are some good reasons why pseudo-two-fold symmetry might be expected. D1 and D2 have structural and sequence similarities to each other (review, Refs. [3,4]). Similarly, CP47 and CP43 appear to be a pair with structural similarities (review, Ref. [45]). These four polypeptides are the largest in the PS II complex and are known to have 1:1:1:1 stoichiometry. Lastly, all of the chlorophyll *a*/*b* binding antennae polypeptides (CP22, CP24, CP26, CP29) are related and are likely to have structures similar to one another [46], introducing still another possibility for pseudosymmetry.

Nonetheless, the evidence that PS II is monomeric is not conclusive. In one case, the evidence is based primarily on a somewhat asymmetric structure with four prominent densities, derived either from a two-dimensional crystal [10] or analysis of single particles [16]. However, the amount of data used to obtain these averages was somewhat sparse and the resolution was 3.0 nm. It has been suggested previously that the structure exhibits pseudo-two-fold symmetry rather than true two-fold symmetry because of the modest resolution [19].

In a second case, a more dimeric structure was obtained, either from two-dimensional crystals of reconstituted PS II preparations [17] or single particle analysis [20]. The conclusion that the structure was pseudo-two-fold symmetric was based primarily on the fact that STEM (scanning transmission electron microscopy) measurements indicated that there was only enough density for a single PS II complex within the entire structure. It was also assumed that these tubular crystals [17] were equivalent to the type 1 crystals from Triton X-100 reported earlier [9]. However, the crystals from the reconstituted PS II preparation [17] clearly resemble the type 3 crystals (Fig. 5) more than the type 1 crystals (Fig. 3). Furthermore, the interpretation of monomer or dimer based on estimations of mass and volume is not without difficulty. The exact polypeptide content of crystals, both with respect to the polypeptides included and the stoichiometry of those polypeptides, is very difficult to determine. Even in very pure prepa-

rations of PS II cores, heterogeneity has been reported to cause problems with crystallization [47,48]. Perhaps, most importantly, the known instability of PS II and the great variation in reported sizes of the complex suggest that structures determined from different preparations are not always comparable with respect to the exact polypeptide content.

The evidence regarding the dimeric nature of PS II is considerably stronger. First, there is biochemical evidence (e.g., Refs. [19,49,50]). Secondly, the conclusion that the structure is dimeric has been supported via completely different structural methods [21]. Thirdly, single particle analysis has revealed 'half-dimers' [18], which have been interpreted as single PS II particles. Two-dimensional crystals of isolated PS II cores (D1, D2, CP47, cytochrome *b*-559) examined by cryoelectron microscopy [15,22] show a monomeric structure which is smaller than the dimeric structure obtained by cryoelectron microscopy of the type 1 crystals [13]. Fourthly, the more recent results from both single particle analyses with much larger data sets [18,24], and two-and three-dimensional analyses of PS II crystals [23] support the dimer model. Lastly, despite the different tubular crystal types observed here and the different detergents used to obtain these crystals, the same apparently dimeric structure was obtained. The type 1 and 2 crystals obtained with the maltoside detergents are at higher resolution than previously obtained and show different crystallographic associations, yet the basic structure is the same. It has been suggested that two-fold symmetry has been improperly imposed on low resolution structures [25]. However, the examination of averages with no symmetry imposed, whether from individual crystals (Fig. 6) or of grand averages derived from several crystals (Fig. 8) also clearly shows two-fold symmetry. Nor were any consistent differences found by difference map analysis of the two halves of the structures.

4.3. Structural summary

A consensus structure is emerging, with PS II arranged as a dimer and each monomer consisting of five major densities [14,23,24,28]. Considerable effort has been made to assign specific polypeptides to each of these densities. However, this effort has been hampered by uncertainty about precisely which polypeptides are included. Even with purified core preparations, it is difficult to be absolutely certain as to which polypeptides have crystallized, as stated previously [22]. As a result, inconsistencies have emerged in the interpretation of the structures obtained. For example, the smallest structures are reported to include CP47, CP43, D1, D2, CP29, CP26, the 33 kDa OEE and four polypeptides below 10 kDa, based on gel electrophoresis of the preparations [17]. In contrast, a larger structure is believed to include only CP47, CP43, D1, D2, cytochrome *b*-559 and a few low molecular polypeptides, based on gel electrophoresis and immunoblots [19,23]. These flat crystals [23] have yielded a structure similar to that obtained from the type 1 and type 2 crystals. Yet, direct antibody labelling on the type 1 crystals has provided evidence that CP29, CP26, CP24 and CP22 are included in the type 1 crystals, in addition to CP47, CP43, D1, D2 and cytochrome *b*-559 [13]. Consequently, caution must be used when extrapolating information regarding polypeptide content from gel electrophoresis of a preparation to a specific structure. Even with direct antibody labelling of the crystals, the stoichiometry per individual dimer is difficult to determine.

Nonetheless, a consensus regarding the location of the RC-CP47 core (D1, D2, cytochrome *b*-559, CP47) is emerging. The most prominent densities are *A* and *B*. Crystals of an RC-CP47 core have been examined and a projection map has been obtained [15]. Areas *A* and *B* appear to be the equivalent of areas 1 and 2 of the RC-CP47 core crystals, with minor extensions into areas *C* and *D*. This interpretation is also consistent with the 0.8-nm map of these same core crystals [22]. A comparison of the structures obtained with RC-CP47 crystals and crystals which also included CP43 has also suggested that the RC-CP47 core is localized primarily to densities *A* and *B* [23]. All of these results are also compatible with earlier antibody labelling results [13], where the COOH-terminal of D1 was localized to density *A* and cytochrome *b*-559 between densities *A* and *B*. There is a projection extending into the central cleft between areas *A* and *B*, and this projection may indicate a close approximation of cytochrome *b*-559 polypeptides across the central depression.

With respect to CP43, recent evidence has suggested that CP43 is located on the periphery, in either

densities *C*, *D* or *E* [23]. Density *C* seems unlikely based on the variability of this area observed in both type 1 and type 2 crystals. Earlier work has suggested that CP43 was localized to density *E* (review, Ref. [28]). More recent work has localized the 23 kDa OEE over density *D* [24]. There is evidence that the 23-kDa polypeptide is closely associated with CP43 (review, Ref. [51]), indicating that density *D* may be the site of CP43. In short, there is not yet a definitive localization with respect to CP43, but it is most likely found in densities *D* or *E*.

It is likely that density *C* and the periphery of the structure around *D* and *E* include some of the minor antennae polypeptides, based on direct immunolabelling of the crystals [13] and the likely location of these polypeptides some distances from the core [52]. This is not in agreement with other models [23,28] where it is proposed that these polypeptides are found only in much larger complexes which are likely to include LHC II [12,19]. However, it is possible that some of the minor antennae polypeptides are found within the structure obtained from the type 1 and type 2 crystals, and that more are included in the larger particles [12,19]. The exact stoichiometry of these polypeptides per reaction center is uncertain [52]. The RC-CP47 structure recently obtained looks quite similar to the dimers found with the type 1 and type 2 crystals, but apparently does not include the minor antennae polypeptides [23]. However, the higher resolution structures shown here (Figs. 6 and 8) clearly have a larger density *E* than the RC-CP47 dimers [23].

Area *C*, and to a much lesser extent, areas *D* and *E*, showed more variations between the halves of the apparent dimer and between crystals. There are several possible interpretations for this. One is that these low density areas are more susceptible to variations in negative staining. However, similar differences in area *C* were noticed when the type 1 crystals were examined by cryoelectron microscopy, with no stain present [13]. It has been known for some time that the antennae polypeptides are more loosely associated with the PS II complexes [52]. If areas *C*, and possibly *E*, as well as the periphery of the structure include the minor antennae polypeptides, differences may be interpreted as the result of inconsistent losses of polypeptides. The type 1 crystals do not include the OEEs [9] and probably do not include the full complement of antennae polypeptides [14], so that inconsistent losses are possible. A further interpretation would be that differences between the low density areas on either half of the dimer indicate that there are slightly different antennae polypeptides associated with each half of the dimer. Notably, areas *A* and *B*, the purported core, showed little variation from crystal to crystal. Also, the fact that no consistent differences were found from crystal to crystal may reflect the reported heterogeneity of PS II with respect to the antennae polypeptides [36,37].

In summary, PS II appears to consist of a dimeric structure with two prominent densities (*A* and *B*) and several low density areas (*C–E*). The high density areas are likely to consist of the RC-CP47 core; CP43 is likely to be found in densities *D* or *E* and a complement of the minor antennae in density *C* and the periphery of the structure.

Acknowledgements

Particular thanks are due to Jim Kremer and Dr. David Mastronarde of the Boulder Laboratory for 3-D Fine Structure for their advice and the use of the image-processing facilities. Thanks to Dr. E.J. Boekema for unpublished information regarding the localization of the 23-kDa polypeptide. This work was supported by NIH #GM40735 (50%) and USDA #9601062 (50%).

References

[1] D.F. Ghanotakis, C.F. Yocum, Photosystem II and the oxygen-evolving complex, Annu. Rev. Plant Physiol. Plant Mol. Biol. 41 (1990) 255–276.

[2] Ö. Hansson, T. Wydrzynski, Current perceptions of photosystem II, Photosynth. Res. 23 (1990) 131–162, N. Adir, M.Y.

[3] R.J. Debus, The manganese and calcium ions of photosynthetic oxygen evolution, Biochim. Biophys. Acta 1102 (1992) 269–352.

[4] W.F.J. Vermaas, S. Styring, W.P. Schröder, B. Andersson, Photosynthetic water oxidation: the protein framework, Photosynth. Res. 38 (1993) 249–263.

[5] L.A. Staehelin, G.W.M. Van der Staay, Structure, composition, functional organization and dynamic properties of thylakoid membranes, in: D.R. Ort, C.Y. Yocum (Eds.), Oxygenic Photosynthesis: the Light Reactions, Kluwer Academic Publishers, Netherlands, 1996, pp. 11–30.

[6] R. Bassi, A.G. Magaldi, G. Tognon, G.M. Giacometti, K.R. Miller, Two-dimensional crystals of the photosystem II reaction center complex from higher plants, Eur. J. Biochem. 50 (1989) 84–93.
[7] J.P. Dekker, S.D. Betts, C.F. Yocum, E.J. Egbert, Characterization by electron microscopy of isolated particles and two-dimensional crystals of the CP47-D1-D2-cytochrome *b*-559 complex of photosystem II, Biochemistry 29 (1990) 3220–3225.
[8] K.R. Miller, J.S. Jacob, Surface structure of the photosystem II complex, 49th Annu. Meeting Elect. Microsc. Soc. America 1991, pp. 196–197.
[9] M.K. Lyon, K.M. Marr, P.S. Furcinitti, Formation and characterization of two-dimensional crystals of photosystem II, J. Struct. Biol. 110 (1993) 133–140.
[10] A. Holzenburg, M.C. Bewley, F.H. Wilson, W.V. Nicholson, R.C. Ford, Three-dimensional structure of photosystem II, Nature 363 (1993) 470–472.
[11] C. Santini, V. Tidu, G. Tognon, A.G. Magaldi, R. Bassi, Three-dimensional structure of the higher-plant photosystem II reaction centre and evidence for its dimeric organization in vivo, Eur. J. Biochem. 221 (1994) 307–315.
[12] E.J. Boekema, B. Hankamer, D. Bald, J. Kruip, J. Nield, A.F. Boonstra, J. Barber, M. Rögner, Supramolecular structure of the photosystem II complex from green plants and cyanobacteria, Proc. Natl. Acad. Sci. U.S.A. 92 (1995) 175–179.
[13] K.M. Marr, D.M. Mastronarde, M.K. Lyon, Two-dimensional crystals of photosystem II: biochemical characterization, cryoelectron microscopy and localization of the D1 and cytochrome *b*-559 polypeptides, J. Cell Biol. 132 (1996) 823–833.
[14] K.M. Marr, R.L. McFeeters, M.K. Lyon, Isolation and structural analysis of two-dimensional crystals of photosystem II from *Hordeum vulgare viridis zb63*, J. Struct. Biol. 117 (1996) 86–98.
[15] K. Nakazato, C. Toyoshima, I. Enami, Y. Inoue, Two-dimensional crystallization and cryoelectron microscopy of photosystem II, J. Mol. Biol. 257 (1996) 225–232.
[16] W.V. Nicholson, F.H. Shepherd, M.F. Rosenberg, R.C. Ford, A. Holzenburg, Structure of photosystem II in spinach thylakoid membranes: comparison of detergent-solubilized and native complexes by electron microscopy, Biochem. J. 315 (1996) 543–547.
[17] G. Tsiotis, T. Walz, A. Spyridaki, A. Lustig, A. Engel, D. Ghanotakis, Tubular crystals of a photosystem II core complex, J. Mol. Biol. 259 (1996) 241–248.
[18] C. Eijekelhoff, J.P. Dekker, E.J. Boekema, Characterization by electron microscopy of dimeric photosystem II core complexes from spinach with and without CP43, Biochim. Biophys. Acta 1321 (1997) 10–20.
[19] B. Hankamer, J. Nield, D. Zheleva, E. Boekema, S. Jansson, J. Barber, Isolation and biochemical characterization of monomeric and dimeric photosystem II complexes from spinach and their relevance to the organisation of photosystem II in vivo, Eur. J. Biochem. 243 (1997) 422–429.
[20] L. Hasler, D. Ghanotakis, B. Fedtke, A. Spyridaki, M. Miller, S.A. Muller, A. Engel, G. Tsiotis, Structural analysis of photosystem II: comparative study of cyanobacterial and higher plant photosystem II complexes, J. Struct. Biol. 119 (1997) 273–283.
[21] R.A. Uphaus, J.Y. Fang, R. Picorel, G. Chumanov, J.Y. Wang, T.M. Cotton, M. Seibert, Langmuir–Blodgett and x-ray diffraction studies of isolated photosystem II reaction centers in monolayers and multilayers—physical dimensions of the complex, Photochem. Photobiol. 65 (1997) 673–679.
[22] K.-H. Rhee, E.P. Morris, D. Zheleva, B. Hankamer, W. Kühlbrandt, J. Barber, Two-dimensional structure of plant photosystem II at 8-Å resolution, Nature 389 (1997) 522–526.
[23] E.P. Morris, B. Hankamer, D. Zheleva, G. Friso, J. Barber, The three-dimensional structure of a photosystem II core complex determined by electron crystallography, Structure 5 (6) (1997) 837–849.
[24] E.J. Boekema, J. Nield, B. Hankamer, J. Barber, Localization of the 23-kDa subunit of the oxygen-evolving complex of photosystem II by electron microscopy, Eur. J. Biochem., 1998, in press.
[25] W.V. Nicholson, R.C. Ford, A. Holzenburg, A current assessment of photosystem II structure, Biosci. Rep. 16 (2) (1996) 159–187.
[26] G. Tsiotis, G. McDermott, D. Ghanotakis, Progress towards structural elucidation of photosystem II, Photosynth. Res. 50 (1996) 93–101.
[27] M. Rögner, E.J. Boekema, J. Barber, How does photosystem 2 split water? The structural basis of efficient energy conversion, TIBS 21 (1996) 44–49.
[28] B. Hankamer, J. Barber, E.J. Boekema, Structure and membrane organization of photosystem II in green plants, Annu. Rev. Plant Physiol. Plant Mol. Biol. 48 (1997) 641–671.
[29] M.F. Schmid, R. Dargahi, M.W. Tam, SPECTRA: a system for processing electron images of crystals, Ultramicroscopy 48 (1993) 251–264.
[30] T.G. Dunahay, L.A. Staehelin, M. Seibert, P.D. Ogilvia, S.P. Berg, Structural, biochemical and biophysical characterization of four oxygen-evolving photosystem II preparations from spinach, Biochim. Biophys. Acta 761 (1984) 179–193.
[31] M. Seibert, M. DeWitt, L.A. Staehelin, Multimeric (tetrameric) particles on the lumenal surface of freeze-etched photosynthetic membranes, J. Cell Biol. 105 (1987) 2257–2265.
[32] W. Kühlbrandt, D.N. Wang, Three-dimensional structure of plant light-harvesting complex determined by electron crystallography, Nature 350 (1991) 130–134.
[33] M. Muller, V.V. Mesyanzhinov, U. Aebi, In vitro maturation of pre-head-like bacteriophage T4 polyheads: structural changes accompanying proteolytic cleavage and lattice expansion, J. Struct. Biol. 112 (1994) 199–215.
[34] A. Brisson, P.N.T. Unwin, Tubular crystals of acetylcholine receptor, J. Cell Biol. 99 (1984) 1202–1211.
[35] R. Henderson, J.M. Baldwin, K.H. Dowing, J. Lepault, F.

Zemlin, Structure of purple membrane from *Halobacterium halobium*: recording, measurement and evaluation of electron micrographs at 3.5 Å resolution, Ultramicroscopy 19 (1986) 147–178.
[36] M. Unser, B.L. Trus, A.C. Steven, A new resolution criterion based on the spectral signal-to-noise ratio, Ultramicroscopy 23 (1987) 39–52.
[37] P.-Å. Albertsson, The structure and function of the chloroplast photosynthetic membrane—a model for the domain organization, Photosynth. Res. 46 (1995) 141–149.
[38] S. Jansson, H. Stefansson, U. Nystrom, P. Gustafsson, P.-Å. Albertsson, Antenna protein composition of PS I and PS II in thylakoid subdomains, Biochim. Biophys. Acta 1320 (1997) 297–309.
[39] G. Horvath, A. Melis, E. Hideg, M. Droppa, L. Vigh, Role of lipids in the organization and function of photosystem II studied by homogeneous catalytic hydrogenation of thylakoid membranes in situ, Biochim. Biophys. Acta 891 (1987) 68–74.
[40] E.M. Aro, I. Virgin, B. Andersson, Photoinhibition of photosystem II: inactivation, protein damage and turnover, Biochim. Biophys. Acta 1143 (1993) 113–134.
[41] Z. Krupa, N.P.A. Huner, J.P. Williams, E. Maissan, D.R. James, Development at cold-hardening temperatures, Plant Physiol. 84 (1987) 19–24.
[42] N.M. Tsvetkova, A.P.R. Brain, P.J. Quinn, Structural characteristics of thylakoid membranes of *Arabidopsis* mutants deficient in lipid fatty acid desaturation, Biochim. Biophys. Acta 1192 (1994) 263–271.
[43] M.F. Schmid, J.P. Robinson, B.R. DasGupta, Direct visualization of botulinum neurotoxin-induced channel in phospholipid vesicles, Nature 364 (1993) 827–830.
[44] B.K. Jap, M. Zulauf, T. Scheybani, A. Hefti, W. Baumeister, U. Aebi, A. Engel, 2-D crystallization: from art to science, Ultramicroscopy 46 (1992) 45–84.
[45] T.M. Bricker, The structure and function of CPa-1 and CPa-2 in photosystem II, Photosynth. Res. 24 (1990) 1–13.
[46] B.R. Green, E. Pichersky, Hypothesis for the evolution of three-helix chl *a* / *b* and chl *a* / *c* light-harvesting antenna proteins from two-helix and four-helix ancestors, Photosynth. Res. 39 (1994) 149–162.
[47] N. Adir, M.Y. Okamura, G. Feher, Crystallization of the PS II-reaction center, in: N. Murata (Ed.), Research in Photosynthesis, Vol. II, Kluwer Publishers, Netherlands, 1992, pp. 195–198.
[48] C. Fotinou, M. Kokkinidis, G. Fritzsch, W. Haase, H. Michel, D.F. Ghanotakis, Characterization of a photosystem II core and its three-dimensional crystals, Photosynth. Res. 37 (1993) 41–48.
[49] G.F. Peter, J.P. Thornber, Biochemical evidence that the higher plant photosystem II core complex is organized as a dimer, Plant Cell Physiol. 32 (1991) 1237–1250.
[50] P. Jahns, H.-W. Trissl, Indications for a dimeric organization of the antenna-depleted reaction center core of photosystem II in thylakoids of intermittent light grown pea plants, Biochim. Biophys. Acta 1318 (1997) 1–5.
[51] A. Seidler, The extrinsic polypeptides of photosystem II, Biochim. Biophys. Acta 1277 (1996) 35–60.
[52] S. Jansson, The light-harvesting chlorophyll *a* / *b* binding proteins, Biochim. Biophys. Acta 1184 (1994) 1–19.